Exploring the Transposition Effects on Electronic and Optics Properties of $Cs_2AgSbCl_6$ Using a Computational-Experimental Approach

Jun Zhou[†,▵] Ximing Rong[‡,▵] Maxim S. Molokeev[§,⊥,□], Xiuwen Zhang[*,‡], Zhiguo Xia[*,†]

[†] The Beijing Municipal Key Laboratory of New Energy Materials and Technologies, School of Materials Sciences and Engineering, University of Science and Technology Beijing, Beijing 100083, China

[‡]Shenzhen Key Laboratory of Micro-Nano Photonic Information Technology, College of Electronic Science and Technology, Shenzhen University, Guangdong 518060, China

[§]Laboratory of Crystal Physics, Kirensky Institute of Physics, Federal Research Center KSC SB RAS, Krasnoyarsk 660036, Russia

[⊥] Siberian Federal University, Krasnoyarsk, 660041, Russia

[□]Department of Physics, Far Eastern State Transport University, Khabarovsk, 680021, Russia

ABSTRACT: The discovery of lead-free double perovskites provides a viable approach in the search for air-stable and environmental benign solar cells absorbers. Inspiring by this, we have now prepared a double perovskite $Cs_2AgSbCl_6$, which is crystallized in cubic unit cell with space group *Fm*-3*m* and is found to have a varied band gap with different body colors. An anti-site defect model was established to investigate transposition influence on the optics and electronic properties of this double-perovskite $Cs_2AgSbCl_6$ structure. Moreover, $Cs_2AgSbCl_6$ perovskite has a high decomposition temperature and is stable upon prolonged exposure to air and moisture, which make it a potential absorber for photovoltaic and optoelectronic applications via further band gap engineering.

■INTRODUCTION

In a remarkably short period of time, Pb-based halide perovskites have launched a new paradigm in the area of solution processable solar cells, surpassing polycrystalline and thin-film silicon photovoltaics, and achieving record power conversion efficiencies above 22%.[1-3] The most extensively studied materials by far are the $APbX_3$ perovskites where A is an alkyl ammonium cation, such as $CH_3NH_3^+$, and X is halide ion (Cl^-, Br^-, I^-).[4-5] Despite their extremely outstanding solar cell performance, the toxicity of lead and the chemical instability of the lead halide perovskites impede their commercialization in the future.[6] Given these limitations, searching for new air-stable and nontoxic lead-free halide perovskites via rational design is one of the key challenges to be addressed in the area of perovskite optoelectronics.[7]

There are different structural design principles adopting in the search for potential Pb-replacements. One straightforward idea to solve the Pb toxicity issue involves replacing Pb^{2+} by Sn^{2+} and Ge^{2+} from the same periodic group, but the chemical instability of Sn^{2+} and Ge^{2+} give rise to limitations for their further utilisation.[8-9] Another promising approach to replace Pb is substitution of more stable cations, Bi^{3+} or Sb^{3+}, which is isoelectronic with Pb^{2+}, show great promise. However, the trivalent vs divalent oxidation state for the metal implies a need for vacancies on the metal site and therefore a lower dimensional structures and wider band gaps for the resulting $A_3M_2VX_9$ (A = K^+, Cs^+, Rb^+, $[NH_4]^+$ and $[CH_3NH_3]^+$); V = vacancy; M = Bi and Sb; X = Cl, Br and I).[10-11]

However, the fact is that there are only a few bivalent or trivalent cations alternative to substitute Pb^{2+} to form stable and non-toxic perovskites.[12] Therefore, another viable route is the combination with a monovalent and a trivalent cation together, which leads to the formation of a double perovskite structure with a basic formula $A_2B'B''X_6$ (A = $CH_3NH_3^+$ or Cs^+; B′ = Na^+, Cu^+ or Ag^+; B″ = Bi^{3+}, Sb^{3+} or In^{3+}; X = Cl^-, Br^-, or I^-).[13-15] The double perovskites have been firstly investigated in the 1970s, initially in the context of ferroelectrics.[16] Recently, in the light of the intense interest in halide perovskites, our group reported $Cs_2AgInCl_6$ with a band gap of 3.23 eV and it can be stable for several weeks in the air.[17] Later, Tran *et al*. successfully control the direct *vs.* indirect nature of the band gap in halide perovskites by $Cs_2AgSb_{1-x}In_xCl_6$ solid solution.[18] Here, we adopt hydrothermal method to grow pure $Cs_2AgSbCl_6$ crystals with varied band gaps, and we established an anti-site defect model by density functional theory (DFT) to investigate transposition influence on the electronic and optics properties of double-perovskite $Cs_2AgSbCl_6$ structure. Moreover, this $Cs_2AgSbCl_6$ crystal was also found to be stable for several weeks in the air and have a high decomposition temperature, which show great potential for photovoltaics and other optoelectronics application via further band gap engineering.

■ EXPERIMENTAL SECTION

Materials and Preparation. All the chemicals were commercially purchased and used without further purification. Crystals $Cs_2AgSbCl_6$ were synthesized by the hydrothermal method in a stainless steel Parr autoclave using 2.4 mmol CsCl, 1.2 mmol AgCl and 1.2 mmol $SbCl_3$ in 0.75 mL HCl acid solution. Powders of different colors from yellow to near black have been precipitated from solution upon heating at 453 K for 12 h. This solid was filtered out and then washed with ethanol and finally dried under reduced pressure overnight.

Characterization. The powder X-ray diffraction (XRD) measurements were conducted on a D8 Advance diffractometer (Bruker Corporation, Germany) operating at 40 kV and 40 mA with Cu Kα radiation (λ = 0.15406 Å), and the scanning rate was fixed at 4°/min. The powder diffraction pattern for Rietveld analysis was collected with the same diffractometer. The step size

of 2θ was 0.016°, and the counting time was 1 s per step. Rietveld refinement was performed by using TOPAS 4.2 software.[19] The morphology and crystalline size of the $Cs_2AgSbCl_6$ samples were determined by scanning electron microscope (SEM, JEOL JSM-6510). Diffuse reflectance spectra were measured on a UV-Vis-NIR spectrophotometer (SHIMADZU UV-3600) attached with an integrating sphere. $BaSO_4$ was used as a reference standard. Thermogravimetric analysis and differential scanning calorimetry (TG–DSC) were performed on a Setaram Labsys Evo at 10 °C min^{-1} in an argon flow from room temperature to 1000 °C.

Computational methods. The band structure of $Cs_2AgSbCl_6$ is calculated by first-principles calculations using density functional theory (DFT), as implemented in the Vienna ab-initio simulation package (VASP) code.[20-21] The projector augmented wave (PAW) potential method was used to describe the interactions between ions and electrons. The exchange–correlation interactions between electrons were treated within the generalized gradient approximation (GGA–PBE).[22-23] The plane wave cut-off energy of 520 eV was used for all total energy calculations and structure optimization and the K-point meshes for different structures were generated according to the Monkhorst–Pack scheme[24] for the Brillouin zones. To reduce the self-interaction error of DFT in band gaps calculations, we used the Heyd - Scuseria - Ernzerhof (HSE) hybrid functional approach[25] to evaluate the band gap and to compare with PBE functional approach.

■ RESULTS AND DISCUSSION

Crystalline Phase and Morphology. Figure 1a displays the observed (black), calculated (red), and the difference (grey) XRD profiles for Rietveld refinement of $Cs_2AgSbCl_6$. It is found that all peaks of the patterns were successfully indexed by cubic cell (*Fm-3m*) with parameters close to $Cs_2AgAuCl_6$ (elpasolite-type structure). As a comparison, site of Au ion in $Cs_2AgAuCl_6$ was occupied by Sb. $Cs_2AgSbCl_6$ belongs to the as-expected lead-free double perovskite, which crystallized in cubic unit cell with space group *Fm*-3*m*, and cell parameters, a = 10.70093 (6), Z = 4. The refinements of $Cs_2AgSbCl_6$ was stable, and the main parameters of processing and refinement with low *R*-factors are provided in Table 1, and the crystallographic information file (CIF) of $Cs_2AgSbCl_6$ is given in the supporting information (SI).

A visualization of the double perovskite structure is presented in Figure 1b, and the fractional atomic coordinates are also given in Table 2. $Cs_2AgSbCl_6$ exhibit a 3-dimensional framework of corner-sharing alternating octahedra of [$AgCl_6$] and [$SbCl_6$], with Cs^+ cations locating in the cavities formed between the octahedra, resulting in a doubled cell, *ie*., elpasolite K_2NaAlF_6 structure, as also observed in $Cs_2AgInCl_6$. The Sb-Cl bond length (2.63(1) Å) is slightly shorter than that of Ag-Cl (2.72(1) Å), as it was expected.

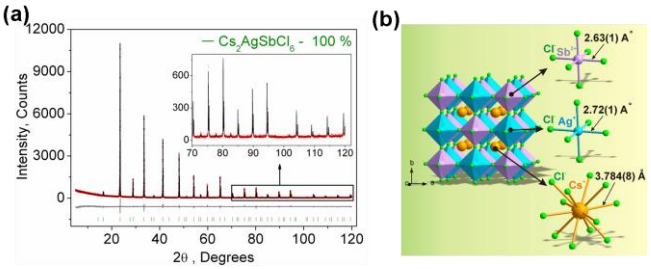

Figure 1. (a) Observed (black), calculated (red), and difference (gray) XRD profiles for the refinement of the $Cs_2AgSbCl_6$ sample using the Rietveld method. (b) Crystal structure of $Cs_2AgSbCl_6$ and coordination environments for Sb^{3+}, Ag^+, and Cl^- are given.

Table 1. Main parameters of processing and refinement of the $Cs_2AgSbCl_6$ sample

Compound	$Cs_2AgSbCl_6$
Sp.Gr.	Fm-3m
a, Å	10.70093 (6)
V, Å3	1225.36 (2)
Z	4
2θ-interval, º	5-120
R_{wp}, %	11.57
R_p, %	8.39
R_{exp}, %	9.40
χ^2	1.23
R_B, %	2.01

Table 2. Fractional atomic coordinates and isotropic displacement parameters (Å2) of $Cs_2AgSbCl_6$

	x	y	z	Biso
Cs	1/4	1/4	1/4	2.71 (9)
Ag	½	1/2	1/2	1.6 (1)
Sb	0	0	0	1.1 (1)
Cl	0.2456 (11)	0	0	3.1 (1)

Figure 2a shows the typical scanning electron microscope (SEM) images of as-prepared $Cs_2AgSbCl_6$ microcrystals, which is comprised of numerous uniform rhombic dodecahedron particles with a size of 15 - 60 μm. A closer observation from the magnified images (Figure 2b) demonstrates that the rhombic dodecahedron shows the typical *fcc*-crystal features, tetradecahedral crystallization habit forming truncated octahedral. Besides, the exhibited facets of $Cs_2AgSbCl_6$ were determined to be (100) and (111).

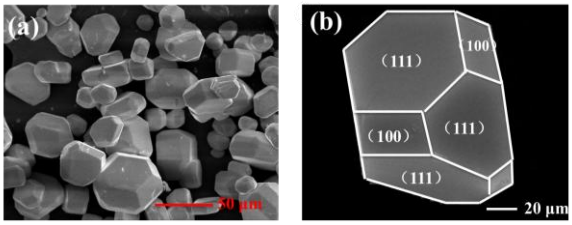

Figure 2. SEM images of $Cs_2AgSbCl_6$ crystals at (a) lower and (b) higher magnification.

It is also worth mentioning that the body colors of the as-prepared powders can be continuously changed from yellow to dark green and eventually to near black under the identical synthetic conditions (Figure 3a). Moreover, all of these samples are of pure phase, and this phenomenon cannot be controlled by the experimental conditions. Therefore, to determine the optical bandgaps for these different colored samples, the UV−vis diffuse reflection spectra of $Cs_2AgSbCl_6$ have been measured. As shown in Figure 3b, as the color of the samples deepens, the reflection curve becomes lower and lower. And the band gap of $Cs_2AgInCl_6$ can be estimated according to eq 1[26]

$$[F(R_\infty)h\nu]^n = A(h\nu - E_g) \quad (1)$$

where $h\nu$ is the photon energy; A is a proportional constant; E_g is the value of the band gap; n = 2 for a direct transition or 1/2 for an indirect transition; and $F(R_\infty)$ is the Kubelka-Munk function defined as[27]

$$F(R_\infty) = (1-R)^2/2R = K/S \quad (2)$$

where R, K, and S are the reflection, absorption, and scattering coefficient, respectively. From the linear extrapolation of $[F(R_\infty)h\nu]^{1/2}=0$ in Figure 3c, we can estimate an indirect optical band gap in the range of 2.61 eV to 2.24 ev with the color changing from yellow to near black.

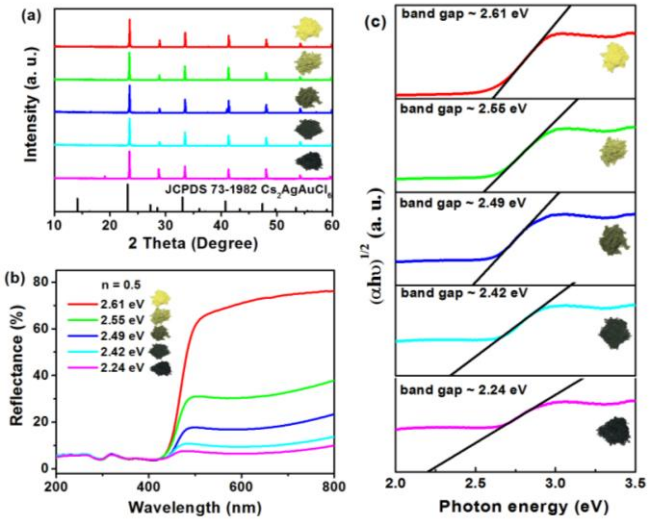

Figure 3. Powder XRD patterns (a), UV-vis diffuse reflectance spectra (b), and Tauc plots (c) of $Cs_2AgSbCl_6$ with very different visible light absorbance.

Band Structure and Optical Absorption Calculations. In order to further investigate this color-tunable phenomenon, we calculated the band structures using density functional theory (DFT). The details of the calculations are available in the Experimental section and the atomic structure used for the calculations is based on the X-ray diffraction data. Figure 4 shows the electronic band structure of double-perovskite $Cs_2AgSbCl_6$ by HSE (a) and PBE (b) calculation. $Cs_2AgSbCl_6$ showed an indirect band gap, with VBM at X (0.5, 0.5, 0) and CBM at L (0.5, 0.5, 0.5). The direct/indirect band gaps of primitive $Cs_2AgSbCl_6$ are 3.33/2.35 eV by HSE and 2.36/1.40 eV by PBE. As the electronic band structures by those two approaches only differ from the band gap, we choose PBE approach to quantitatively describe the defect influence on the electronic and optical properties of $Cs_2AgSbCl_6$ in the following investigations.

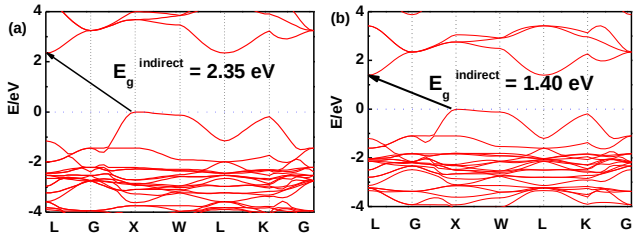

Figure 4. Electronic band structure of double-perovskite $Cs_2AgSbCl_6$ by HSE (a) and PBE (b) approach.

Since Ag and Sb have rather similar local environments in the present cubic double-perovskite $Cs_2AgSbCl_6$ phase, (e.g. $Ag[Cl_6Cs_8Sb_6Ag_{12}]$ and $Sb[Cl_6Cs_8Ag_6Sb_{12}]$ that differ only at the third shell, and similar atomic radii (0.16 nm for Ag and for 0.145 nm for Sb[28])), it is worthwhile to study the anti-site defect between them. Furthermore, because we considered the anti-site defect with swapped Ag and Sb atoms, the ratio of every element will not be changed, making the defect structures possibly allomorphic. Figure 5a shows a diagrammatic sketch of two anti-site defect models of $Cs_2AgSbCl_6$ structures based on a primitive (with rhombic structure) enlarged 2 × 2 × 2 super cell ($Cs_{16}Ag_8Sb_8Cl_{48}$). In these two anti-site models, an Ag atom makes atomic transposition with its nearest neighbor (NN) Sb and second-nearest neighbor (2NN) Sb atom. Before selecting the size of the super cell, we tested the size effect of the defect energy, as shown in Figure 5b. For NN and 2NN structures, E_{defect} has been converged according with the results of 2 × 2 × 2 and 3 × 3 × 3 super cells, meaning that the 2 × 2 × 2 super cell is large enough to avoid boundary effect caused by DFT calculation. And the structural parameters of primitive $Cs_2AgSbCl_6$ and 3 $Cs_{16}Ag_8Sb_8Cl_{48}$ (balanced, NN and 2NN) structures after full relaxation are shown in Table 3. Comparing with the balanced structures, the lattice of NN and 2NN defect structures expanded and the total energy were increased by 0.625 eV (NN) and 0.975 eV (2NN) due to the internal defect influenced in the lattice. For NN anti-site model, the structure is no longer rhombic, this is mainly because the transposition occurred within the diagonal of the face rather than the body diagonal, causing the lattice expanding uncoordinated with a distortion. For 2NN anti-site model, the lattice is also slightly expanded (by 0.39%). Due to the relatively low formation energy of anti-site defects (e.g. 0.625 eV for NN anti-site), a significant amount of Ag-Sb anti-site defects would form. The Ag and Sb anti-site defects would be connected to their NN, 2NN, 3NN, … neighboring anti-sites in the crystal.

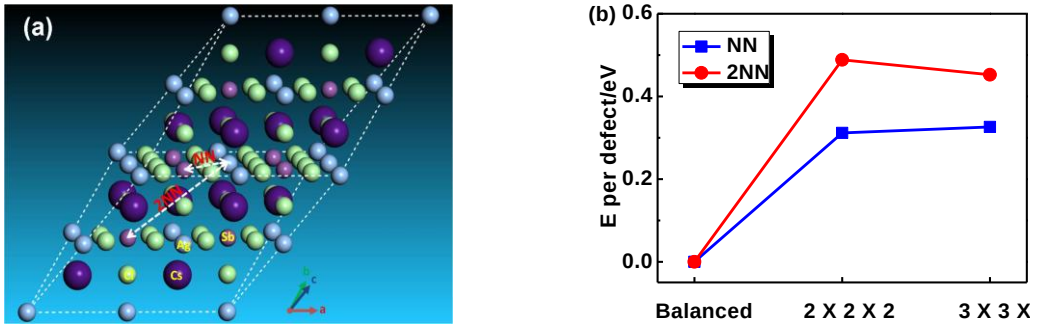

Figure 5. (a) Diagrammatic sketch of two anti-site defect models of $Cs_2AgSbCl_6$ structures. NN: transposition of Ag and its nearest neighbor Sb atom; 2NN: transposition of Ag and its second-nearest neighbor Sb atom. (b) Energy per defect for NN and 2NN structures for $2\times2\times2$ and $3\times3\times3$ $Cs_2AgSbCl_6$ super cells.

Table 3. Structural parameters of primitive $Cs_2AgSbCl_6$ and 3 $Cs_{16}Ag_8Sb_8Cl_{48}$ (balanced, NN and 2NN) structures.

Structure	E_{tot}(eV)	ΔE(eV)	ΔE/atom(meV)	V(Å^3)	L_a(Å)	L_b(Å)	L_c(Å)	α(°)	β(°)	γ(°)
Primitive	-32.703	--	--	319	7.672	7.672	7.672	60	60	60
Balanced	-261.625	0	0	2554	15.343	15.343	15.343	60	60	60
NN	-261.000	0.625	7.81	2586	15.397	15.424	15.397	59.94	60.12	59.94
2NN	-260.650	0.975	12.19	2584	15.403	15.403	15.403	60	60	60

Figure 6 shows the electronic band structures of NN (Fig. 6a) and 2NN (Figure 6b) $Cs_{16}Ag_8Sb_8Cl_{48}$ anti-site structures from the PBE calculations, respectively. The direct band gaps of the anti-site structures are decreased from 2.36 eV (pristine) to 1.36 eV (NN) and 1.13 eV (2NN). The decreasing of the direct gap from NN to 2NN anti-sites reflects the effect of the local electric field between the oppositely charged Ag and Sb anti-site defects. Details of band gaps are presented in Table 4. As NN and 2NN are allotropies of double-perovskite $Cs_2AgSbCl_6$ structures, the obvious gap differences indicate that this defect model could stand a good chance in the experiments.

Figure 6c shows the imaginary part of the dielectric functions of 3 $Cs_{16}Ag_8Sb_8Cl_{48}$ structures. The absorption edges as coincided with the direct band gaps (see Table 4), showed $E_{balanced} > E_{NN} > E_{2NN}$, which are in consist with the band gap variation of these structures. As we discussed before, since a significant amount of anti-sites with NN, 2NN, … nearest neighbor configurations would form at the experimental temperature, $Cs_2AgSbCl_6$ would have strong optical absorption for photons with energy much lower than its pristine optical band gap. It would be hard to define strictly the actual optical gap of defective $Cs_2AgSbCl_6$. However, the optical absorbance of defective $Cs_2AgSbCl_6$ to visible light (below its optical band gap of ~3.33 eV according to HSE calculations) can be continuously varied due to the formation of anti-site defects. Indeed, in experiment, we observed almost continuously constant optical absorbance for most visible light in $Cs_2AgSbCl_6$ below its pristine optical band gap (see Fig. 3b) indicated by a clear optical absorption shoulder that doesn't change much for different samples (the variation of optical gap from 2.61 to 2.24 eV could not explain the significant variation of sample colors). The main different between the samples with different colors is the magnitude of reflectance for visible light (see the right side of Fig. 3b), i.e. the darker sample absorbs (reflects) more (less) visible light. A possible reason is that the darker sample contains more Ag-Sb anti-site defects. The above optical absorption feature is rather different than the widely studied tune-ability of sample color by controlling sizes of nano-crystals (e.g. in Ref. [29]), where the optical absorption shoulder changes significantly for different samples with different nano-crystal sizes. In our experiments, we also observed slight variation of optical absorption shoulders, which may reflect the change of nano-crystal sizes. Furthermore, although there are contributions from phonon assistant absorption in Fig. 3b, phonon effect could not explain the sharp variation of sample colors since phonon assistant absorption could not go below the fundamental gap of pristine $Cs_2AgSbCl_6$ (2.35 eV according to HSE calculations) much. The tune-ability of visible light absorbance in $Cs_2AgSbCl_6$ induces variety of colors of the materials, and could have further implications for optical properties.

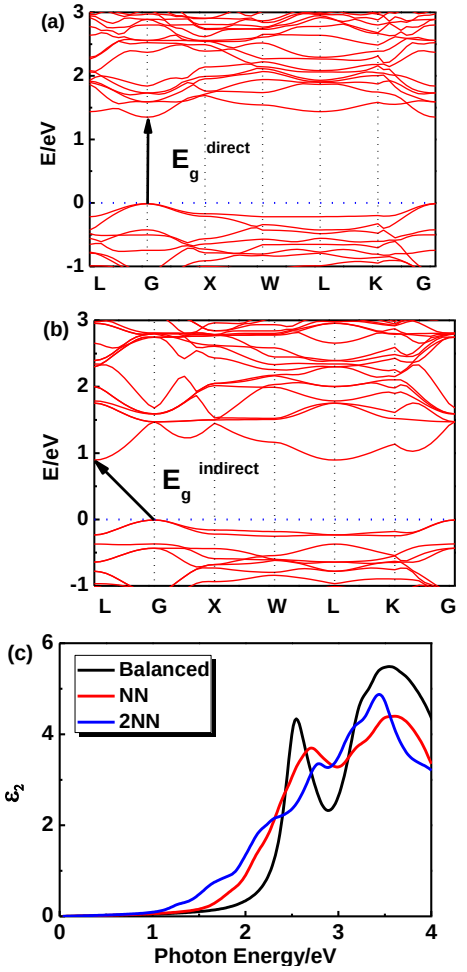

Figure 6. Electronic band structure of NN (a) and 2NN (b) $Cs_{16}Ag_8Sb_8Cl_{48}$ anti-site structures from the PBE calculations. (c) Imaginary part of the dielectric functions of 3 $Cs_{16}Ag_8Sb_8Cl_{48}$ structures from the PBE calculations.

Table 4. Band gap of $Cs_2AgSbCl_6$ for different anti-site defect models and calculating methods

Structure	Calculating method	E_g^{direct}/eV	$E_g^{indirect}$/eV	$E_g^{overall}$/eV
Primitive	HSE	3.33	2.35	2.35
Primitive	PBE	2.36	1.40	1.40
NN	PBE	1.36	--	1.36
2NN	PBE	1.13	0.90	0.90

Chemical, Light and Thermal Stability. Regarding the environmental stability of $Cs_2AgSbCl_6$, the selected $Cs_2AgSbCl_6$ sample with 2.61 eV were exposed to the ambient atmosphere in both light and moisture conditions, with the powder XRD and UV−vis diffuse reflectance spectroscopy monitored as a function of time (Figure 7). It is found that there is nearly no apparent difference on the thermal and chemical stability depending on the crystal size. Hence, as can be seen in Figure 7a, the powder XRD patterns for one month' storage (in the ambient atmosphere) show no evidence of material decomposition, indicating that the material is rather stable. As for the reflectance spectrum, no obvious change was detected in the curve shape except for the slight intensity decline (Figure 7b).

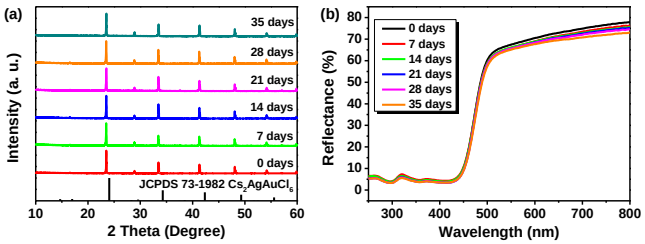

Figure 7. PXRD patterns (a) and UV-vis diffuse reflectance spectra (b) of $Cs_2AgSbCl_6$ after 0 days, 7 days, 14 days, 21 days, 28 days and 35 days of exposure to light and moitsure conditions.

Halide perovskites are known for low decomposition and formation energies. Since thermal stability is also an important parameter for halide perovskites in the prospective applications, we carried out thermogravimetric and differential scanning calorimetry (TG–DSC) analysis of a $Cs_2AgSbCl_6$ powder sample (Figure 8), with weight loss occurring in three steps. The first process with the small weight loss, observed at around 200 °C, is connected to the release of adsorbed water from the sample surface. Furthermore, the second weight loss is 28.55 wt%, which mainly occurred from 250 to 500 °C. Herein, the obvious exothermic peak shown on the DSC curve is centered at about 356 °C, which is ascribed to the evaporation of $SbCl_3$. Notable, $SbCl_3$ constitutes 32.21% of the total weight in $Cs_2AgSbCl_6$, and therefore, the decomposition reaction equation might be described as follows: $Cs_2AgSbCl_6 \rightarrow SbCl_3 + Cs_2AgCl_3$. Finally, the third serious weight loss of 42.64 wt%, observed at 500 – 1000 °C and centered at around 756 °C, is attributed to the evaporation of CsCl, which corresponds to 47.55% of the total weight in $Cs_2AgSbCl_6$, and the decomposition process could proceed according to the scheme below: $Cs_2AgCl_3 \rightarrow AgCl + 2CsCl$.[30] The above results showed that $Cs_2AgSbCl_6$ is relatively stable to mass loss up to 250 °C. After that, some obvious decomposition reaction occurs enabling the materials lose the functionality completely.

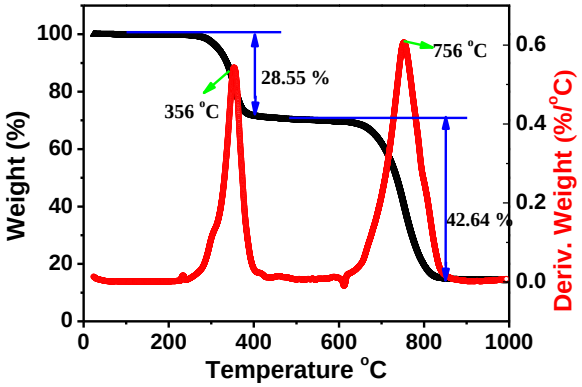

Figure 8. TGA and DSC data for a powder sample $Cs_2AgSbCl_6$.

■CONCLUSION

In summary, we have designed and prepared the phase pure $Cs_2AgSbCl_6$ crystals by the hydrothermal routes, which is relatively stable and non-toxic and has a low band gap. To demonstrate the transposition influence on the electronic and optics properties of $Cs_2AgSbCl_6$, focusing a combined experimental and theoretical study, we established an anti-site defect model by density functional theory (DFT). By exchanging site-equal Ag and Sb, the two allotropies (NN and 2NN) are thermodynamically stable with only 7~12 meV/atom larger than balanced structure, and the band gap could be relatively varied with rarely small lattice expansion. Overall, the discovery of $Cs_2AgSbCl_6$ furthermore stress on the importance of the double perovskite approach in the search for lead-free photovoltaic materials that exhibit good stability.

AUTHOR INFORMATION

Corresponding Author

* E-mail: xiuwenzhang@szu.edu.cn (X. Zhang)
* E-mail: xiazg@ustb.edu.cn (Z. Xia)

Author Contributions

[Δ]These authors contributed equally.

Notes

The authors declare no competing financial interests.

ACKNOWLEDGMENT

The present work was supported by the National Natural Science Foundation of China (Grants 91622125 and 51572023), Natural Science Foundations of Beijing (2172036), and National Key R&D Program of China (Grant 2016YFB0700700), and M. Molokeev acknowledges support of the Russian Foundation for Basic Research (17-52-53031).

REFERENCES

(1). Seo, J.; Noh, J. H.; Seok, S. I., Rational strategies for efficient perovskite solar cells. *Acc. Chem. Res.* **2016,** *49* (3), 562-72.

(2). Kojima, A.; Teshima, K.; Shirai, Y.; Miyasaka, T., Organometal halide perovskites as visible-light sensitizers for photovoltaic cells. *J. Am. Chem. Soc.* **2009,** *131* (17), 6050-6051.

(3). Jeon, N. J.; Noh, J. H.; Kim, Y. C.; Yang, W. S.; Ryu, S.; Seok, S. I., Solvent engineering for high-performance inorganic-organic hybrid perovskite solar cells. *Nat. Mater.* **2014,** *13* (9), 897-903.

(4). Stranks, S. D.; Eperon, G. E.; Grancini, G.; Menelaou, C.; Alcocer, M. J.; Leijtens, T.; Herz, L. M.; Petrozza, A.; Snaith, H. J., Electron-hole diffusion lengths exceeding 1 micrometer in an organometal trihalide perovskite absorber. *Science* **2013,** *342* (6156), 341-344.

(5). Yokoyama, T.; Cao, D. H.; Stoumpos, C. C.; Song, T. B.; Sato, Y.; Aramaki, S.; Kanatzidis, M. G., Overcoming short-circuit in lead-free $CH_3NH_3SnI_3$ perovskite solar cells via kinetically controlled gas-solid reaction film fabrication process. *J. Phys. Chem. Lett.* **2016,** *7* (5), 776-82.

(6). Volonakis, G.; Filip, M. R.; Haghighirad, A. A.; Sakai, N.; Wenger, B.; Snaith, H. J.; Giustino, F., Lead-free halide double perovskites via heterovalent substitution of noble metals. *J. Phys. Chem. Lett.* **2016,** *7* (7), 1254-9.

(7). Giustino, F.; Snaith, H. J., Toward lead-free perovskite solar cells. *ACS Energy Lett.* **2016,** *1* (6), 1233-1240.

(8). Stoumpos, C. C.; Frazer, L.; Clark, D. J.; Kim, Y. S.; Rhim, S. H.; Freeman, A. J.; Ketterson, J. B.; Jang, J. I.; Kanatzidis, M. G., Hybrid germanium iodide perovskite semiconductors: active lone pairs, structural distortions, direct and indirect energy gaps, and strong nonlinear optical properties. *J. Am. Chem. Soc.* **2015,** *137* (21), 6804-19.

(9). Hao, F.; Stoumpos, C. C.; Cao, D. H.; Chang, R. P. H.; Kanatzidis, M. G., Lead-free solid-state organic-inorganic halide perovskite solar cells. *Nat. Photonics.* **2014,** *8* (6), 489-494.

(10). Xiao, Z. W.; Meng, W. W.; Wang, J. B.; Mitzi, D. B.; Yan, Y. F., Searching for promising new perovskite-based photovoltaic absorbers: the importance of electronic dimensionality. *Mater. Horiz.* **2017,** *4* (2), 206-216.

(11). Sun, S. J.; Tominaka, S. S.; Lee, J. H.; Xie, F.; Bristowe, P. D.; Cheetham, A. K., Synthesis, crystal structure, and properties of a

perovskite-related bismuth phase, $(NH_4)_3Bi_2I_9$. *APL Mater.* **2016,** *4* (3), 31101.
(12). Cheng, P. F.; Wu, T.; Li, Y. J.; Jiang, L.; Deng, W. Q.; Han, K. L., Combining theory and experiment in the design of a lead-free ($(CH_3NH_3)_2AgBiI_6$) double perovskite. *New J. Chem.* **2017,** *41* (18), 9598-9601.
(13). Zhao, X. G.; Yang, J. H.; Fu, Y.; Yang, D.; Xu, Q.; Yu, L.; Wei, S. H.; Zhang, L., Design of lead-free inorganic halide perovskites for solar cells via cation-transmutation. *J. Am. Chem. Soc.* **2017,** *139* (7), 2630-2638.
(14). McClure, E. T.; Ball, M. R.; Windl, W.; Woodward, P. M., Cs_2AgBiX_6(X = Br, Cl): New Visible Light Absorbing, Lead-Free Halide Perovskite Semiconductors. *Chem. Mater.* **2016,** *28* (5), 1348-1354.
(15). Vasala, S.; Karppinen, M., $A_2B'B''O_6$ perovskites: A review. *Prog. Solid State Chem.* **2015,** *43* (1-2), 1-36.
(16). Morss, L. R.; Siegal, M.; Stenger, L.; Edelstein, N., Preparation of cubic chloro complex compounds of trivalent metals: Cs_2NaMCl_6. *Inor. Chem.* **1970,** *9* (7), 1771-1775.
(17). Zhou, J.; Xia, Z. G.; Molokeev, M. S.; Zhang, X. W.; Peng, D. S.; Liu, Q. L., Composition design, optical gap and stability investigations of lead-free halide double perovskite $Cs_2AgInCl_6$. *J. Mater. Chem. A.* **2017,** *5* (29), 15031-15037.
(18). Tran, T. T.; Panella, J. R.; Chamorro, J. R.; Morey, J. R.; McQueen, T. M., Designing indirect–direct bandgap transitions in double perovskites. *Mater. Horiz.* **2017,** *4* (4), 688-693.
(19). TOPAS, V., 2: General profile and structure analysis software for powder diffraction data–User's Manual; Bruker AXS: Karlsruhe, Germany. 2008. *There is no corresponding record for this reference* **2002**.
(20). Kresse, G.; Hafner, J., Ab initiomolecular dynamics for liquid metals. *Phys. Rev. B* **1993,** *47* (1), 558-561.
(21). Kresse, G.; Furthmüller, J., Efficient iterative schemes for ab initio total-energy calculations using a plane-wave basis set. *Phys. Rev. B* **1996,** *54* (16), 11169.
(22). Blöchl, P. E., Projector augmented-wave method. *Phys. Rev. B* **1994,** *50* (24), 17953-17979.
(23). Perdew, J. P.; Burke, K.; Ernzerhof, M., Generalized gradient approximation made simple. *Phys. Rev. Lett.* **1996,** *77* (18), 3865.
(24). Monkhorst, H. J.; Pack, J. D., Special points for Brillouin-zone integrations. *Phys. Rev. B* **1976,** *13* (12), 5188-5192.
(25). Krukau, A. V.; Vydrov, O. A.; Izmaylov, A. F.; Scuseria, G. E., Influence of the exchange screening parameter on the performance of screened hybrid functionals. *J. Chem. Phys.* **2006,** *125* (22), 224106.
(26). Zhou, J.; Xia, Z. G.; Bettinelli, M.; Liu, Q. L., Photoluminescence tuning via energy transfer in Eu-doped $Ba_2(Gd,Tb)_2Si_4O_{13}$ solid-solution phosphors. *RSC Adv.* **2016,** *6* (3), 2046-2054.
(27). Xia, Z. G.; Zhang, Y. Y.; Molokeev, M. S.; Atuchin, V. V., Structural and luminescence properties of yellow-emitting $NaScSi_2O_6:Eu^{2+}$ phosphors: Eu^{2+} site preference analysis and generation of red emission by codoping Mn^{2+} for white-light-emitting diode applications. *J. Phys. Chem. C* **2013,** *117* (40), 20847-20854.
(28). Slater, J. C., Atomic Radii in Crystals. *J. Chem. Phys.* **1964,** *41* (10), 3199-3204.
(29). Malgras, V.; Tominaka, S.; Ryan, J. W.; Henzie, J.; Takei, T.; Ohara, K.; Yamauchi, Y., Observation of quantum confinement in monodisperse methylammonium lead halide perovskite nanocrystals embedded in mesoporous silica. *J. Am. Chem. Soc.* **2016**.
(30). Emmenegger, F. P., Gaseous complexes—Their role in chemical transport. *J. Cryst. Growth.* **1972,** *17*, 31-37.